THE JOURNAL OF PHYSICAL CHEMISTRY B LETTERS

2006, *110,* 9759−9763
Published on Web 05/03/2006

Periodic Inclusion of Room-Temperature-Ferromagnetic Metal Phosphide Nanoparticles in Carbon Nanotubes

Vincent Jourdain,*,†,‡ Edward T. Simpson,§ Matthieu Paillet,† Takeshi Kasama,§,|| Rafal E. Dunin-Borkowski,§,|| Philippe Poncharal,† Ahmed Zahab,† Annick Loiseau,⊥ John Robertson,‡ and Patrick Bernier†

LCVN, UMR 5587 CNRS-UM2, Université Montpellier II, Place Bataillon, CC26, 34095 Montpellier Cedex 5, France, Department of Engineering, University of Cambridge, Trumpington Street, Cambridge CB2 1PZ, UK, Department of Materials Science & Metallurgy, University of Cambridge, Pembroke Street, Cambridge CB2 3QZ, UK, Frontier Research System, The Institute of Physical and Chemical Research, Hatoyama, Saitama 350-0395, Japan, and LEM, UMR 104 CNRS-ONERA, ONERA, BP 72, 92322 Châtillon Cedex, France

Received: February 24, 2006; In Final Form: April 22, 2006

We demonstrate the use of sequential catalytic growth to encapsulate iron, nickel−iron, and iron−cobalt phosphide catalyst nanoparticles periodically along the entire lengths of carbon nanotubes. Investigations by local electron spectroscopies and electron diffraction reveal the compositions and crystal structures of the encapsulated particles. Significantly, high spatial resolution magnetic characterization using magnetic force microscopy and off-axis electron holography demonstrates that encapsulated iron−cobalt phosphide nanoparticles are ferromagnetic at room temperature, in accordance with the properties of bulk metal phosphides of the same structure and composition.

Introduction

Carbon nanotubes that contain encapsulated magnetic nanoparticles have potential applications in magnetic storage,[1] spin-polarized scanning tunneling microscopy,[2] and the emerging field of spintronics.[3] The desirable properties of carbon nanotubes for such applications include their nanoscale size, the possibility of ballistic transport at room temperature, and a high spin coherence length.[1,4,5] In principle, the combination of carbon nanotubes with ferromagnetic materials enables both the injection and the manipulation of highly polarized spin currents.[6] Since the discovery of carbon nanotubes,[7] numerous compounds have been inserted into their inner channels.[8−16] However, control of the encapsulated crystal localization, size, and shape has proved to be challenging.

To date, the sequential catalytic growth (SCG) mechanism is the only method that has been demonstrated to allow the synthesis of carbon nanotubes that have regularly spaced nanoparticles encapsulated along their entire lengths.[17] The SCG mechanism is based on the use of phosphorus as a catalytic poison, which induces a kinetic mismatch between carbon supply and consumption. This mitmatch generates a periodic fluctuation of the carbon concentration in the catalyst particle, which manifests itself in the form of periodic initiations and interruptions of the growth. Fractions of the catalyst particle are encapsulated regularly at each new initiation. In this process, the spacing between successive particles depends on the carbon supply and on the size of the primary catalyst particle. A potential drawback of this approach is that it requires the use of a metal phosphide catalyst. As a result, the inserted compounds are metal phosphides and not pure metals, which complicates their use as room-temperature ferromagnets, although several binary and ternary metal phosphides can be ferromagnetic in certain composition domains, with Curie temperatures of up to 700 K.[18,19] The only catalyst that was initially found to be suitable for SCG was the ternary Ni−Fe−P alloy.[20]

Here, we show that iron phosphides and (iron, cobalt) phosphides can also be used to induce the SCG of carbon nanotubes that contain periodically inserted crystals. We use local electron spectroscopies and electron diffraction to characterize the compositions and crystal structures of the inserted nanoparticles, and magnetic force microscopy (MFM) and off-axis electron holography to determine their magnetic properties with sub-10 nm spatial resolution. Significantly, our results show that the SCG mechanism can be used to grow carbon nanotubes that contain regularly spaced room-temperature-ferromagnetic nanoparticles.

Experimental Details

Thin metal (nickel, iron, cobalt) layers were evaporated onto anodic alumina membranes (AAMs) (Anodisc Whatman, 0.02 μm). The nanofilaments are grown at the surface of these supported metal layers by catalytic decomposition of carbon precursors at high temperature. Most important is that commercial AAMs intrinsically contain ∼1.5 at. % phosphorus (as

* Corresponding author. E-mail: jourdain@lcvn.univ-montp2.fr.
† Université Montpellier II.
‡ Department of Engineering, University of Cambridge.
§ Department of Materials Science & Metallurgy, University of Cambridge.
|| The Institute of Physical and Chemical Research.
⊥ LEM.

10.1021/jp061181f CCC: $33.50

measured by EDX), resulting from their oxidation process by phosphoric acid. We previously demonstrated that phosphorus diffuses into the metal layer during the heating ramp to form the metal phosphide nanoparticles that are responsible for the SCG mechanism.[17,20] Optimal growth conditions to induce the growth of periodically inserted carbon nanotubes from Fe and Fe−Co layers were found to be 76 sccm CH_4/730 sccm H_2 at 1150 °C. In comparison, carbon nanotubes periodically inserted by Ni−Fe phosphide particles were grown from an 80 nm Ni/20 nm Fe layer (80Ni−20Fe), using the previously reported growth conditions:[20] 134 sccm CH_4/730 sccm H_2 at 1080 °C. The resulting nanofilament morphologies were characterized by transmission electron microscopy (TEM) (JEOL 1200 EX2, 100 kV), using carbon-coated grids that had been dipped in suspensions of the nanofilaments in ethanol. Nanoparticle compositions were studied using energy-dispersive X-ray spectroscopy (EDX) in a Philips CM20 TEM (200 kV) and electron energy-loss spectroscopy (EELS) in a Philips CM300-ST TEM (300 kV). High-resolution electron microscopy (HREM) and electron diffraction (JEOL 4000FX, 400 kV) were used to study the crystal structures of the nanoparticles. MFM measurements were performed using a Digital Instruments Dimension 3100 NSIIIa, with a CoCr-coated etched silicon probe tip (length ∼225 μm, resonant frequency ∼70 kHz, spring constant ∼1−5 N/m). The lift height for interleave scans in the MFM was 50 nm. Off-axis electron holograms were acquired at 300 kV using a Philips CM300-ST TEM equipped with a Lorentz lens and an electron biprism. A biprism voltage of 200 V was used to form holographic fringes of spacing 3.25 nm. In situ magnetization reversal allowed holographic phase images to be acquired after the sample had been saturated magnetically in opposite directions. Differences between these phase images were used to isolate the magnetic contribution to the phase shift, with all mean inner potential contributions to the phase shift removed.[21]

Results and Discussion

In the present study, we focus on iron−cobalt phosphides because these compounds have more favorable ferromagnetic properties than other metal phosphides at room temperature (see below).[18,19] The TEM image in Figure 1a shows the morphology of nanofilaments that were grown using 90 nm Fe/10 nm Co (90Fe−10Co). The filaments exhibit a distinctive periodic "matchstick" morphology, characteristic of the SCG mechanism,[17] with the end of each "match" filled by an ellipsoidal nanoparticle whose volume is a fraction of that of the primary catalyst particle. In previously reported SCG syntheses (using Ni−Fe catalysts), ∼95% of the nanotubes had a periodic structure and ∼80% of the elementary units encapsulated a nanoparticle.[20] In the case of the Fe−Co catalyst, the encapsulation yield is virtually 100% (see Supporting Information). This difference may result from a better wetting of the graphene surface at the higher temperature used for Fe−Co phosphide catalysts (1150 °C instead of 1080 °C), but additional data is required to support this explanation. The optimal growth temperature for 90Fe−10Co was 1150 °C, which is noticeably higher than that for 80Ni−20Fe (1080 °C). This temperature is consistent with the need for the catalyst particles to be in a liquid state.[20] A typical SCG nanotube contains more than one hundred nanoparticles encapsulated in sequence. Both the sizes of the encapsulated particles and their separations decrease slowly along the length of each filament. The particles can be described as ellipsoids that have the same symmetry axis as the nanotubes. The nanoparticle length l (along the nanotube symmetry axis)

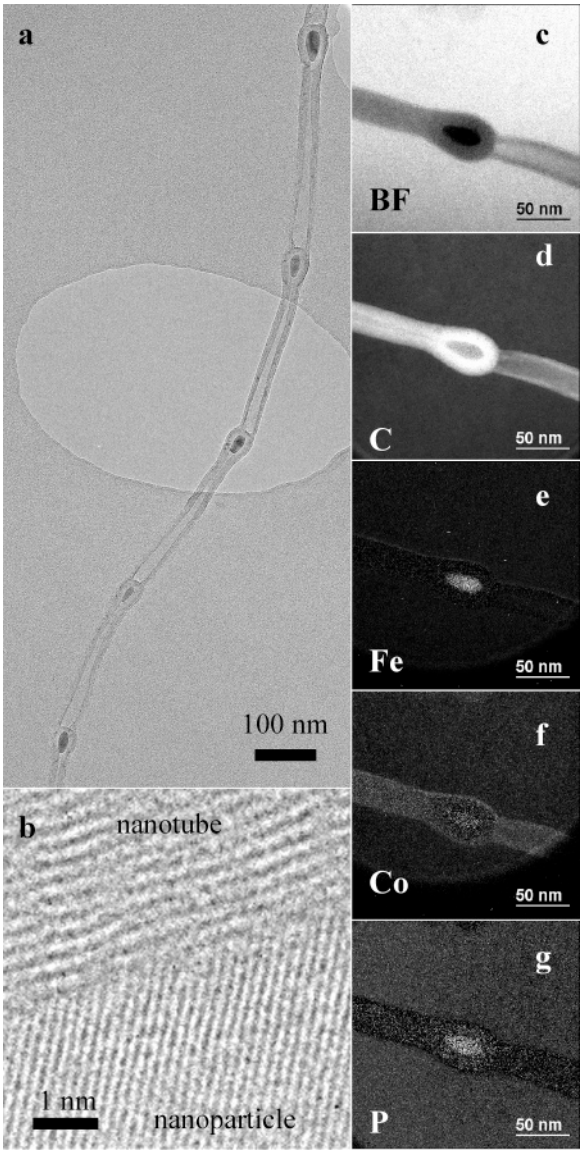

Figure 1. (a) TEM image of a carbon nanotube periodically inserted with Fe−Co−P nanoparticles. (b) HRTEM image of an encapsulated Fe−Co−P nanoparticle. (c) Bright field zero loss and (d−g) EELS energy filtered elemental maps for (d) carbon, (e) iron, (f) cobalt, and (g) phosphorus of an encapsulated Fe−Co−P nanoparticle.

typically ranges from 100 to 25 nm, and the nanoparticle width w (perpendicular to the nanotube symmetry axis) from 60 to 10 nm (see Supporting Information). Their aspect ratio (l/w) can vary from 1.5 to 4 between particles, without any systematic trend. Along a given filament, the distance between particles diminishes progressively from typically 1 μm to 100 nm. The Ni−P, Co−P, and Fe−P binary phase diagrams all have a eutectic point at a phosphorus concentration of ∼17−20 at. %, but their eutectic temperatures are 870 °C for Ni−P, 1023 °C for Co−P, and 1048 °C for Fe−P.

For both Ni−Fe−P and Fe−Co−P, EELS and energy-selected imaging confirmed that the nanoparticles comprised an alloy of two metals and phosphorus, as shown in Figures 1c−g for an Fe−Co−P particle. Although diffraction contrast sometimes affected the chemical maps for large (>50 nm) particles, and although artifacts sometimes affected the maps as a result of overlapping edges in the EELS spectrum, ∼90% of the particles examined were found to be homogeneous in composition. This homogeneity is in good accordance with our initial compositional analyses of the Ni−Fe−P nanoparticles

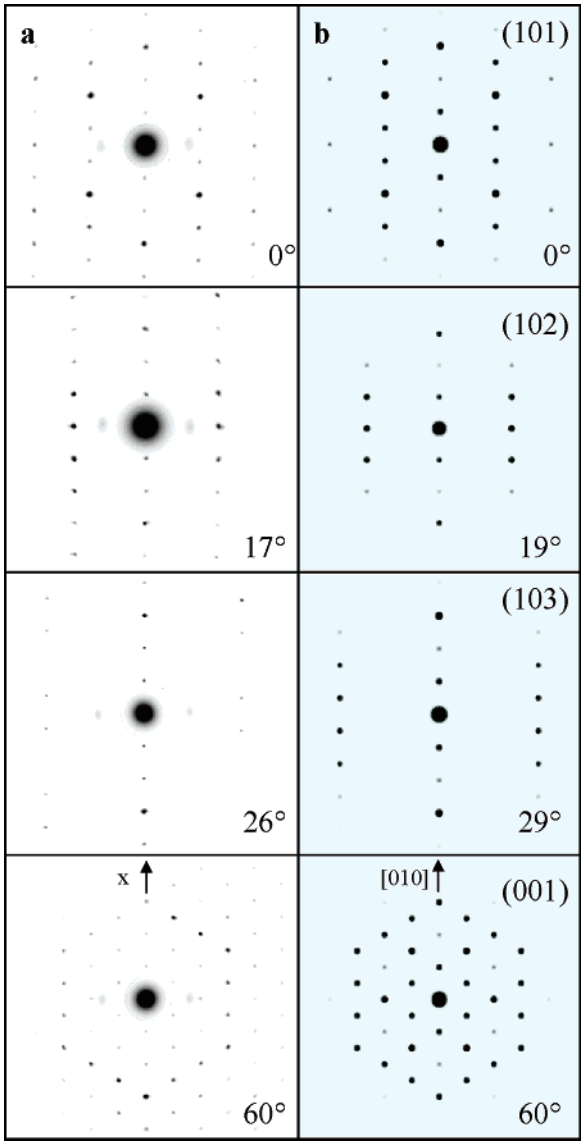

Figure 2. (a) Experimental electron diffraction patterns of a 50 × 108 nm Ni−Fe−P nanoparticle. (b) Simulated diffraction patterns for a crystal with the Fe_2P structure. The angles of rotation about the [010] vertical axis are indicated.

using spatially resolved EELS with a 5Å probe, as reported elsewhere.[17] Quantitative EDX analyses were used to provide values for the nanoparticle compositions of Ni/Fe/P ∼ 45/28/27 at. % for 80Ni−20Fe and Fe/Co/P ∼ 55/14/31 at. % for 90Fe−10Co. Close to these compositions, the phase diagrams suggest that the following crystal structures are possible: hexagonal "Fe_2P" (or "Ni_2P"), orthorhombic "Co_2P", hexagonal "Ni_5P_2", tetragonal "$Ni_{12}P_5$", and tetragonal "Fe_3P" (or "Ni_3P"). HRTEM revealed that most of the particles were single crystals (lower part of Figure 1b), although the largest crystals could contain several distinct grains. In addition, HRTEM evidenced that the filament walls are made of well-defined graphene layers parallel to the particle surface (upper part of Figure 1b). The crystal structure varied between particles within a given filament, usually between "Fe_2P" and "Fe_3P" structures. The left side of Figure 2 shows representative experimental electron diffraction patterns acquired from a single encapsulated crystal, for different rotation angles about one symmetry axis (labeled *x*). The diffraction patterns can be attributed to an Fe_2P-type crystal structure by comparison with simulated patterns for an Fe_2P crystal in different orientations about its [010] axis (right side of Figure 2). Simulations were calculated using the code CRYSTALDIFFRACT within the kinematical theory.

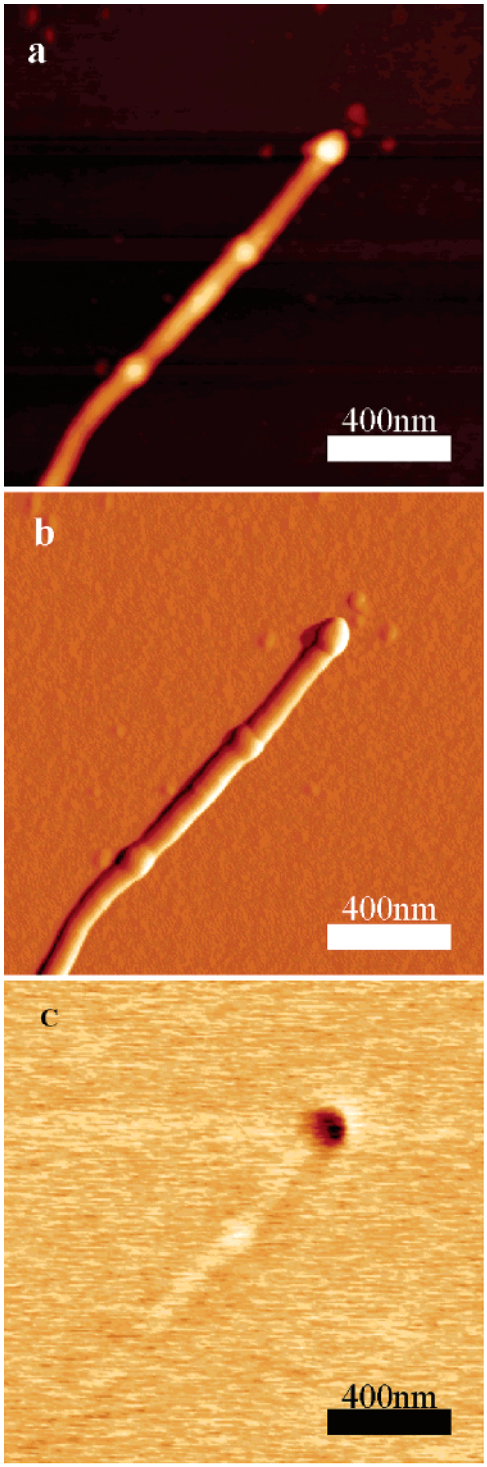

Figure 3. (a) Topography, (b) amplitude, and (c) MFM images of a nanotube periodically encapsulating Fe−Co−P nanoparticles.

The magnetic properties of both the encapsulated Ni−Fe−P and Fe−Co−P particles were initially studied at room temperature using MFM. The positions of the encapsulated particles could be determined easily in AFM mode (Figure 3a,b), thanks to the presence of local increases in the widths of the nanotubes (see Figure 1). While MFM measurements did not show a magnetic signal from any Ni−Fe−P particles (data not shown), strong magnetic contrast was observed from the largest Fe−Co−P particles (with combined nanotube widths in excess of 60 nm), which were typically found at the ends of filaments

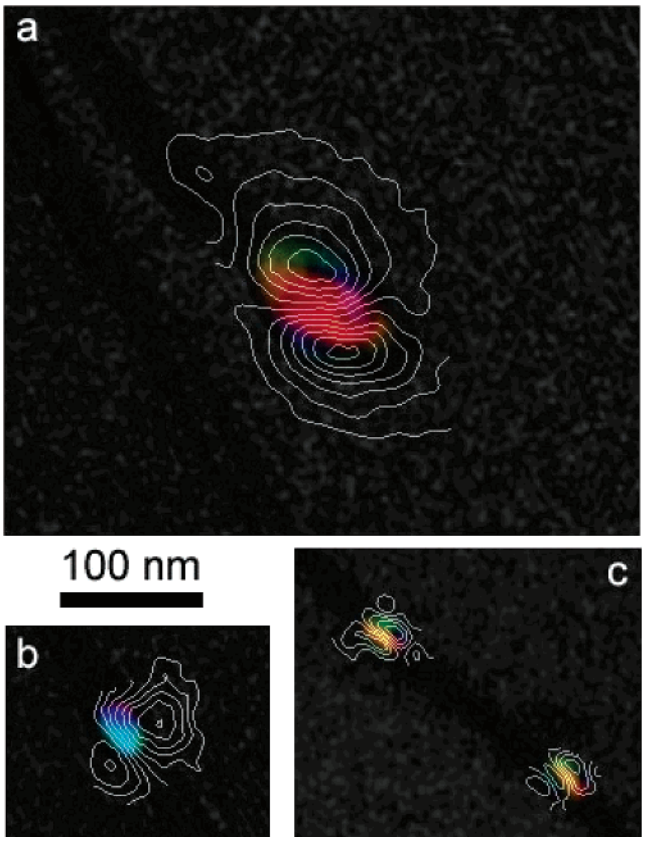

Figure 4. (a) Magnetic induction map overlaid onto an amplitude image of a 52 × 98 nm Fe−Co−P nanoparticle. Contour spacing is 0.125 rad. (b) As for Figure 4a, but a smaller particle (40 × 16 nm, contour spacing 0.125 rad), more representative of those found periodically inserted into nanotubes. (c) Two periodically spaced particles in a nanotube, of a similar size to the one shown in Figure 4b. Contour spacing 0.06 rad.

(Figure 3c). No magnetic contrast was observed from the smallest particles, for which the combined nanotube width was below 60 nm, as measured by AFM. TEM observations indicate that combined widths in excess of 60 nm typically correspond to nanoparticles with dimensions greater than $l \times w \sim 60 \times 30$ nm. To determine whether this lack of contrast resulted from the detection limit of the technique or from the superparamagnetic limit of the nanoparticles, off-axis electron holograms of the samples were acquired. This technique, which allows the phase shift of the electron wave that has passed through a specimen to be measured in the TEM, is noninvasive and allows the magnetic induction in the specimen to be recorded in transmission rather than close to its surface. Unwanted contributions to the measured phase shift from variations in mean inner potential were removed by using the conventional TEM objective lens to saturate each catalyst particle magnetically parallel and then antiparallel to its long axis. The magnetic contribution to the phase shift was obtained by determining half of the difference between phase images that were acquired with the catalyst particles magnetized in opposite directions, with the objective lens turned off and the sample at remanence. Contours were added to the resulting magnetic phase images to reveal the magnetic flux density in the specimen quantitatively. This procedure is described in detail elsewhere.[22] Electron holography was used to confirm that the largest Fe−Co−P nanoparticles were ferromagnetic at room temperature, as shown in Figure 4a for a $l \times w = 98 \times 52$ nm ellipsoidal Fe−Co−P nanoparticle. Both the (slightly "S"-shaped) magnetic flux distribution in the particle and the return flux around it confirm that it is ferromagnetic. This particle has an "Fe_2P" crystal structure (as determined by HRTEM), with its [001] easy axis of magnetization parallel to the observed phase contours but 30° out of the specimen plane. The phase shift across this particle is approximately 1.5 rad, corresponding to a magnetic flux density of between 0.5 and 0.8 T, assuming that the particle is magnetized throughout its measured diameter, with the range of values reflecting different possible particle geometries and inclinations of the magnetization from the specimen plane. This value is in good agreement with the expected value for an Fe_2P crystal (see below). Particles of intermediate size (typically down to $l \times w \sim 40 \times 15$ nm) were also found to be ferromagnetic at room temperature: Figures 4b,c show magnetic induction maps obtained from 40 × 15 nm encapsulated ferromagnetic particles. For substantially smaller particles, the signal-to-noise ratio was too low to allow their magnetic properties to be determined with confidence from single pairs of holograms. For Ni−Fe−P particles, electron holography performed using the same procedure confirmed the absence of a measurable ferromagnetic signal at room temperature from particles of any size.

These results are in good agreement with the known magnetic properties of the bulk metal phosphides $(Fe_{1-x}, M_x)_2P$ and $(Fe_{1-x}, M_x)_3P$ (M = Ni, Co). Fe_3P is ferromagnetic, with a Curie temperature of ∼700 K and a saturation magnetic moment of 122 $\mu_B \cdot nm^{-3}$, corresponding to a magnetic flux density of 1.4 T. For comparison, bulk iron has a saturation magnetic moment of 187 $\mu_B \cdot nm^{-3}$. The substitution of a small amount of Fe by Co ($x < 0.4$) does not modify these properties substantially, whereas substitution by Ni decreases the Curie temperature and the magnetic moment dramatically.[19] Fe_2P is ferromagnetic, with a Curie temperature of 265 K and a saturation magnetic moment of 80 $\mu_B \cdot nm^{-3}$, corresponding to a magnetic flux density of 0.93 T. The substitution of a small amount of Fe by Co or Ni results in a significant increase in the Curie temperature to above room temperature, up to 342 K for $x_{Ni} = 0.08$ and up to 459 K for $x_{Co} = 0.38$.[18] For higher concentrations of Ni or Co, the Curie temperature decreases dramatically to below room temperature. The addition of Ni is therefore generally detrimental to the ferromagnetic properties of such crystals, while, over a large range of Co compositions, both "Fe_2P" and "Fe_3P"-type compounds are ferromagnetic at room temperature. These properties are in good agreement with our local magnetic measurements for the different compositions of metal phosphide nanoparticles and explain why a ferromagnetic signal can be observed from Fe−Co−P particles at room temperature, but not from Ni−Fe−P particles. A detailed study of the influence of particle structure, orientation, shape, and separation on magnetic properties will be published elsewhere.

It is worth mentioning that our initial efforts to determine the magnetic properties of the encapsulated nanoparticles by conventional (SQUID) magnetometry were hindered by contamination of the bulk samples by metal particles outside the nanotubes. These particles originated from the deposited metal layer, during the ultrasonic treatment necessary to detach the nanotubes from their macroscopic support (anodic alumina). A significant aspect of this study is that, in contrast to conventional macroscopic magnetic measurements, which may be influenced by metal catalyst contamination outside the nanotubes, the magnetic properties of the encapsulated particles were determined unambiguously by local characterization at the nanometer scale.

Conclusion

In conclusion, we have demonstrated that the SCG mechanism can be used to encapsulate room-temperature-ferromagnetic

nanoparticles periodically in carbon nanotubes. Over the measured range of particle sizes, the encapsulated nanoparticles have saturation magnetizations that are close to those expected for bulk metal phosphides of the same structure and composition. When compared with previously reported methods, SCG has the advantage of allowing the encapsulation, along the entire length of each nanotube, of regularly spaced nanoparticles that have well-defined sizes and shapes. Since the periodicity of the particles is correlated directly with the instantaneous growth conditions,[17] SCG is also important for achieving a high degree of structural control over the final composite structures.

Acknowledgment. This work was supported by the Marie Curie Intra-European Fellowship Program (project "ArchiTech'Tube"). R.E.D. and E.T.S. thank the Royal Society and the EPSRC, respectively, for financial support. Part of this work was supported by the GDR-E NanoE (N°2756) of the CNRS.

Supporting Information Available: (S1) Distribution of the nanoparticles length and width ($N = 73$); (S2a,b) Low magnification TEM images of Co−Fe−P samples. This material is available free of charge via the Internet at http://pubs.acs.org.

References and Notes

(1) Kuo, C. T.; Lin, C. H.; Lo, A. Y. *Diamond Relat. Mater.* **2003**, *12*, 799.

(2) Bode, M.; Getzlaff, M.; Wiesendanger, R. *Phys. Rev. Lett.* **1988**, *81*, 4256.

(3) Wolf, S. A.; Awschalom, D. D.; Buhrman, R. A.; Daughton, J. M.; von Molnàr, S.; Roukes, M. L.; Chtchelkanova, A. Y.; Treger, D. M. *Science* **2001**, *294*, 1488.

(4) Tsukagoshi, K.; Alphenaar, B. W.; Ago, H. *Nature* **1999**, *401*, 572.

(5) Tsukagoshi, K.; Alphenaar, B. W.; Wagner, M. *Mater. Sci. Eng., B* **2001**, *84*, 26.

(6) Yang, C.-K.; Zhao, J.; Lu, J. P. *Phys. Rev. Lett.* **2003**, *90*, 257403-1.

(7) Iijima, S. *Nature* **1991**, *354*, 56.

(8) Seraphin, S.; Zhou, D.; Jiao, J.; Withers, J. C.; Loufty, R. *Nature* **1993**, *362*, 503.

(9) Dujardin, E.; Ebbesen, T.; Hiura, H.; Tanigaki, K. *Science* **1994**, *265*, 1850.

(10) Ajayan, P. M.; Ebbesen, T.; Ichihashi, T.; Iijima, S.; Tanigaki, K.; Hiura, H. *Nature* **1993**, *362*, 522.

(11) Ajayan, P. M.; Iijima, S. *Nature* **1993**, *361*, 333.

(12) Tsang, S. C.; Chen, Y. K.; Harris, P. J. F.; Green, M. L. H. *Nature* **1994**, *372*, 159.

(13) Hsu, W. K.; Hare, J. P.; Terrones, M.; Kroto, H. W.; Walton, D. R. M. *Nature* **1995**, *377*, 687.

(14) Liang, C. H.; Meng, G. W.; Zhang, L. D.; Shen, N. F.; Zhang, X. Y. *J. Cryst. Growth* **2000**, *218*, 136.

(15) Leonhardt, A.; Ritschel, M.; Kozhuharova, R.; Graff, A.; Muhl, T.; Huhle, R.; Monch, I.; Elefant, D.; Schneider, C. M. *Diamond Relat. Mater.* **2003**, *12*, 790.

(16) Elias, A. L.; Rodriguez-Manzo, J. A.; McCartney, M. R.; Golberg, D.; Zamudio, A.; Baltazar, S. E.; Lopez-Urias, F.; Munoz-Sandoval, E.; Gu, L.; Tang, C. C.; Smith, D. J.; Bando, Y.; Terrones, H.; Terrones, M. *Nano Lett.* **2005**, *5*, 467.

(17) Jourdain, V.; Stéphan, O.; Castignolles, M.; Loiseau, A.; Bernier, P. *Adv. Mater.* **2004**, *16*, 447.

(18) Fruchart, R.; Roger, A.; Senateur, J. P. *J. Appl. Phys.* **1969**, *40*, 1250.

(19) Goto, M.; Tange, H.; Tokunaga, T.; Fujii, H.; Okamoto, T. *Jpn. J. Appl. Phys.* **1977**, *16*, 2175.

(20) Jourdain, V.; Paillet, M.; Almairac, R.; Loiseau, A.; Bernier, P. *J. Phys. Chem. B* **2005**, *109*, 1380.

(21) Dunin-Borkowski, R. E.; McCartney, M. R.; Smith, D. J. Electron holography of nanostructured materials. In *Encyclopaedia of Nanoscience and Nanotechnology*; Nalwa, H. S., Ed; American Scientific Publishers: Stevenson Ranch, California, 2004; Vol. 3, pp 41−100.

(22) Dunin-Borkowski, R. E. D.; Kasama, T.; Wei, A.; Tripp, S. L.; Hÿtch, M. J.; Snoeck, E.; Harrison, R. J.; Putnis, A. *Microscopy Res. Technol.* **2004**, *64*, 390.